Frequency Analysis of Linearly Coupled Modes of MEMS Arrays

Prashant N.Kambali, Gyanadutta Swain, and Ashok Kumar Pandey*
Department of Mechanical and Aerospace Engineering,
Indian Institute of Technology Hyderabad, Medak Dist-502285, India.

Abstract

Microelectromechanical system, MEMS, based arrays have been employed to increase the bandwidth and sensitivity of many sensors and actuators. In this paper, we present an approximate model to demonstrate the tuning of in-plane and out-of-plane frequencies of MEMS arrays consisting of fixed-fixed beams. Subsequently, we apply the Galerkin's method with single approximate mode to obtain the reduced order static and dynamic equations. Corresponding to a given DC voltage, we first solve the static equations and then obtain corresponding frequencies from the dynamic equation for single beam and arrays of multibeams. We compare the model with available experimental results. Later, we show the influence of different frequency tuning parameters such as the initial tensions, fringing field coefficients and the variable inter beam gaps between the microbeam and electrodes to control the coupling region and different modal freqencies of the beam. Finally, we obtain a compact model which can be used in optimizing the bandwidth and sensitivity of microbeams array.

1 Introduction

Microelectromechanical (MEMS) or nanoelectromechanical system (NEMS) based arrays have gained increased interest for their potential applications as sensors and actuators due to high sensitivity and high bandwidth. Recent studies reveal that the sensitivity as well as frequency bandwidth of a resonant sensor or an actuator can be improved using different frequency tuning mechanisms [1, 2, 3, 4, 5, 6, 7, 8]. Among these, the most commonly used techniques are tuning by electrostatic dc biasing, thermal stressing, structural hardening, etc. In this paper, we deal with frequency tuning due to dc bias in an array of microbeams.

There have been many experimental and theoretical studies in the literature which describe the tuning of coupled modes and coupling regions. Suzuki *et al.* [1] have proposed a method of electrostatic frequency tuning in a fish bone shaped MEMS resonator to study the coupling of first five modes. Spletzer *et al.* [2] studied vibration localization of mechanically coupled identical microcantilevers in large arrays for ultrasensitive mass detection and identification.

*Address all correspondence to this author. E-mail: ashok@iith.ac.in

Verbridge *et al.* [4] employed chip-bending method to control tensile stress in doubly clamped nanomechanical beam resonators. They showed that this technique provides the ability to tune both frequency and quality factor. Pandey *et al.* [5] tuned tension of the beam due to temperature change to induce the variation in linear frequency. Remtema and Lin [6] have adopted the frequency tuning using localized thermal stressing effect on comb shaped micro resonator. Buks and Roukes [7] have applied the method of electrostatic tuning to an array of 67 fixed-fixed microbeam resonators made of Au and described the significance of collective response of inplane modes. Later, Kozinsky *et al.* [8] have used the electrostatic frequency tuning mechanism to tune nonlinear and linear frequency of inplane and out-of-plane motion in order to increase the dynamic range of a NEMS resonator consists of a single fixed-fixed beam which is separated from a side electrode and a bottom electrode, respectively. Solanki *et al.* [9] experimentally showed the existence of mode mixing region in nanowire resonator. Zalalutdinov *et al.* [12] studied collective modes in two dimensional arrays using a double laser setup with independent positioning of the point laser drive and interferometric motion detector. Krylov *et al.* [13] demonstrated the coupling effect of out-of-plane modes in an array of cantilever beams due to parametric excitation. Thijssen *et al.* [14] demonstrated the frequency tuning of in-plane modes of an array of nanobeams under the optical excitation by varing the width of each beam. Kambali and Pandey [15] demonstrated tunning of nonlinear frequency response of electrostatically excited microbeam subjected to direct and fringing fields. Gutschmidt and Gottlieb [17, 16] investigated internal resonance and bifurcations in an array of nonlinearly coupled microbeams subjected to parametric excitation. Pandey [18] theoretically modeled the frequency tuning of in-plane and out-of-plane modes and their coupled effect of NEMS device and compared the result with experiments from Kozinsky *et al.* [8]. However, he did not consider the fringing effects in the electrostatic forces which resulted in the mismatching of theoretical results with experimental values. Furthuremore, he also showed that the mode mixing of two or more modes plays very important role in increasing the operating frequency range. In this paper, we present frequency analysis of an array of multibeam.

Recently, we have presented the experimental analysis of the coupling of in-plane as well as out-of-plane modes of single and multibeam arrays [19]. Using the exact mode shape, we have also presented the theoretical prediction of intermodal coupling. However, the theoretical analysis presented in [19] is very complex (see supplementary material [19]), hence, it is difficult to be used as an effective design tool for optimizing the various parameters associated with arrays such as the gap between the beams, distance between the beams and bottom electrode, tension in the beams, fringing effects, etc. Therefore, in this paper, we present theoretical model of frequency tuning based on approximate mode shapes of in-plane and out-of-plane modes of microbeam arrays. Unlike the previous model, the resultant theoretical model clearly shows the coupled and non-coupled terms of the modes of same beam or neighboring beams. After validating the developed model based on approximate modes with the experimental results from [19] for single beam and array of three beams, we discuss different cases of the coupling of three-beams array due to changes in side gaps, bottom gap, fringing coefficients and initial tensions, respectively.

2 Governing Equations

To develop the mathematical model based on the approximate modes of in-plane and out-of-plane motions for N clamped−clamped beams, we consider the array configuration as shown in Figure 1. Figure 1 shows an array of N clamped-clamped beams each having length L, width B and thickness H, which are separated from each other by air gaps of g_0,g_1,g_3 ,...,g_n with two fixed side electrodes E_1 and E_2 on either side of the array, respectively. The beams are also separated from the bottom electrode E_g by a gap of d. Taking the deflection of the beam along in-plane and out-of-plane direction as $y(x,t)$ and $z(x,t)$, respectively, as shown in Figure 2(a), the equation of motion for two modes of each beam after considering residual tension and mid-plane stretching [20] can be written as

$$EI_{\bar{z}}\bar{y}_n^{''''} + \rho A\ddot{\bar{y}}_n - \left[N_{n0} + \frac{EA}{2L}\int_0^L \left(\bar{z}_n^{'2} + \bar{y}_n^{'2}\right)d\bar{x}_n\right]\bar{y}_n^{''} = Q_{n\bar{y}}(\bar{y},\bar{z},\bar{t}) \tag{1}$$

$$EI_{\bar{y}}\bar{z}_n^{''''} + \rho A\ddot{\bar{z}}_n - \left[N_{n0} + \frac{EA}{2L}\int_0^L \left(\bar{z}_n^{'2} + \bar{y}_n^{'2}\right)d\bar{x}_n\right]\bar{z}_n^{''} = Q_{n\bar{z}}(\bar{y},\bar{z},\bar{t}) \tag{2}$$

where, subscript prime and dot represent differentiation with respect to x and t, respectively, N_{n0} is the initial tension induced in each beam by fabrication processes [10, 11], heating [5, 19], etc., with $n = 1, 2, ..., N$, E is the Young's modulus of the beam, EI is the bending rigidity, $I_z = HB^3/12$, $I_y = BH^3/12$ are area moment of inertia about z and y-axes, and ρ is the material density. The boundary conditions for the fixed-fixed beam are taken as

$$\bar{y_n}(0,t) = \bar{y_n}(L,t) = 0, \bar{z_n}(0,t) = \bar{z_n}(L,t) = 0, \bar{y}_n^{'}(0,t) = \bar{y}_n^{'}(L,t) = 0 \bar{z}_n^{'}(0,t) = \bar{z}_n^{'}(L,t) = 0. \tag{3}$$

The forcing Q_y and Q_z are the effective electrostatic forces per unit length along y and z directions for single beam configuration as shown in Figure 2. Similarly, Q_{ny} and Q_{nz} are the corresponding effective electrostatic forces per unit length along y and z directions for n^{th} beam. The forcing are based on parallel plate capacitor assumptions which consider direct as well as fringing field effects in both y and z directions [19]. The expressions for the forcing are given by

$$Q_{n\bar{y}}(\bar{y},\bar{z},\bar{t}) = \frac{1}{2}k_1\epsilon_0 H\left[\frac{\left(V_{(n)(n-1)} + v(t)\right)^2}{\left(g_{(n-1)} + \bar{y}_{(n-1)} - \bar{y}_{(n)}\right)^2} - \frac{\left(V_{(n)(n+1)} + v(t)\right)^2}{\left(g_n + \bar{y}_n - \bar{y}_{(n+1)}\right)^2}\right] \tag{4}$$

$$\begin{aligned} Q_{n\bar{z}}(\bar{y},\bar{z},\bar{t}) = {} & \frac{1}{2}\frac{{V_{(n)(g)}}^2\epsilon_0}{B^2\left(d-\bar{z_n}\right)^2}\left[4.32\,b^3 + 0.0182\,b\big(d-\bar{z_n}\big)^2 - k_2 0.00068\,\left(d-\bar{z_n}\right)^3\right] \\ & -\frac{1}{2}\frac{\epsilon_0 H}{gB^2}\big(k_3 0.156\bar{z_n} + 0.0049B\big)\left[\left(V_{(n)(n-1)} + v(t)\right)^2 + \left(V_{(n)(n+1)} + v(t)\right)^2\right] \end{aligned} \tag{5}$$

where, $\epsilon_0 = 8.85 \times 10^{-12}$ F/m is the vacuum permittivity. Here, k_1 contributes for the net effect of fringing and direct fields in y-direction, k_2 and k_3 represent the strength of the fringing field effects from the bottom electrode and two side electrodes on the z-direction deflection. $V_{ij} = V_i - V_j$ is the difference in the DC voltage applied between the beam and electrodes.

2.1 Non-Dimensional Equation

Taking the ratio of the beam and side electrode gaps as $r_n = (g_n/g_0)$, we rescale the equations of motion using the variables $x_n = \bar{x_n}/L$, $y_n = \bar{y_n}/g$, $z_n = \bar{z_n}/d$, $t = \bar{t}/T$, where, $T = \sqrt{\rho A L^4/EI_z}$. Thus, the non-dimensional equation of motion for two modes of each beam in an array can be written as

$$y_n^{''''} + \ddot{y}_n - [N_n + \alpha_1\Gamma(y_n, y_n) + \alpha_2\Gamma(z_n, z_n)]y_n^{''} = \beta_s\left[\frac{(V_{(n)(n-1)} + v(t))^2}{(r_{n-1} + y_{n-1} - y_n)^2} - \frac{(V_{(n)(n+1)} + v(t))^2}{(r_n + y_n - y_{n+1})^2}\right] \quad (6)$$

$$z_n^{''''} + \alpha_3\ddot{z}_n - \alpha_3[N_n + \alpha_1\Gamma(y_n, y_n) + \alpha_2\Gamma(z_n, z_n)]z_n^{''} = (\beta_g + \beta_{2g}(1 - z_n)^2 - \beta_{3g}(1 - z_n)^3)$$
$$\frac{(V_{(n)(g)} + v(t))^2}{(1 - z_n)^2} - (\alpha_g + \alpha_{2g}z_n)[(V_{(n)(n-1)} + v(t))^2 + (V_{(n)(n+1)} + v(t))^2]. \quad (7)$$

where, the terms associated with the above equations are defined as

$$\Gamma(p(x_n, t), q(x_n, t)) = \int_0^1 \frac{\partial p}{\partial x_n}\frac{\partial q}{\partial x_n}\mathrm{d}x_n, N_n = \frac{N_{n0}L^2}{EI_z}, \alpha_1 = \frac{6g^2}{B^2}, \alpha_2 = \frac{6d^2}{B^2}, \alpha_3 = \left(\frac{I_z}{I_y}\right),$$
$$\beta_s = \frac{6k_1\sigma_1}{B^3g^3}, \beta_g = \frac{25.92\sigma_1}{H^3d^3}, \beta_{2g} = \frac{0.1092\sigma_1}{B^2H^3d}, \beta_{3g} = \frac{k_2 4.08\times10^{-3}\sigma_1}{H^3B^3}, \alpha_g = \frac{0.0294\sigma_1}{gB^2H^2d},$$
$$\alpha_{2g} = \frac{k_3 9.36\times10^{-1}\sigma_1}{gB^3H^2}, \sigma_1 = \frac{\epsilon_0 L^4}{E}. \quad (8)$$

The nondimensional boundary conditions can also be written as subjected to following sets of boundary conditions

$$y_n(0,t) = y_n(1,t) = 0, \quad z_n(0,t) = z_n(1,t) = 0, \quad y_n^{'}(0,t) = y_n^{'}(1,t) = 0, \quad z_n^{'}(0,t) = z_n^{'}(1,t) = 0 \quad (9)$$

2.2 Static and Dynamic Equation

The net beam deflection under electrical force is composed of a static deflection due to the DC voltage and a dynamic deflection due to the AC voltage. Therefore, the deflection in the y and z directions due to static and dynamic components of the electrical force are given by

$$y_n(x,t) = u_{ns}(x) + u_n(x,t),$$
$$z_n(x,t) = w_{ns}(x) + w_n(x,t). \quad (10)$$

The static deflections $u_{ns}(x)$ and $w_{ns}(x)$ are obtained by substituting Eqn. (10) in Eqns. (6) and (7) and subsequently setting the time derivatives and dynamic displacements $u_n(x,t)$ and $w_n(x,t)$ equal to zero. The resulting static equations are found as

$$u_{ns}^{''''} - [N_n + \alpha_1\Gamma(u_{ns}, u_{ns}) + \alpha_2\Gamma(w_{ns}, w_{ns})]\, u_{ns}^{''} = \beta_s\left[\frac{(V_{(n)(n-1)})^2}{(r_{n-1} + u_{(n-1)s-u_{ns}})^2}\right.$$
$$\left. - \frac{(V_{(n)(n+1)})^2}{(r_n + u_{ns} - u_{(n+1)s})^2}\right] \quad (11)$$

$$w_{ns}^{''''} - \alpha_3\,[N_n + \alpha_1\Gamma(u_{ns}, u_{ns}) + \alpha_2\Gamma(w_{ns}, w_{ns})]\, w_{ns}^{''} = (\beta_g + \beta_{2g}(1 - w_{ns})^2 - \beta_{3g}(1 - w_{ns})^3)$$
$$\frac{(V_{(n)g})^2}{(1 - w_{ns})^2} - \alpha_g[(V_{(n)(n-1)})^2 + (V_{(n)(n+1)})^2] + \alpha_{2g}[(V_{(n)(n-1)})^2(w_{(n-1)s} - w_{ns})$$
$$+(V_{(n)(n+1)})^2(w_{(n+1)s} - w_{ns})] \quad (12)$$

The corresponding dynamic deflections $u_n(x,t)$ and $w_n(x,t)$ are obtained by substituting Eqn. (10) in Eqns. (6) and (7). Using u_{ns}'''' and w_{ns}'''' from Eqns. (11) and (12) and expanding the forcing terms about $u_n = 0$ and $w_n = 0$ upto the first order, we get nonlinear dynamic equations. In order to get the linear dynamic equations, we neglect the nonlinear terms and dynamic forcing terms from resulting nonlinear dynamic equations. Hence, the linear dynamic equations can be written as

$$u_n'''' + \ddot{u}_n - \Big[2\alpha_1\Gamma(u_{ns},u_n) + 2\alpha_2\Gamma(ws,w)\Big]u_{ns}'' - \Big[N_n + \alpha_1\Gamma(u_{ns},u_{ns}) + \alpha_2\Gamma(w_{ns},w_{ns})\Big]u_n'' = 2\beta_s\Big[(V_{(n)(n-1)})^2\frac{u_n - u_{n-1}}{(r_{n-1} + u_{(n-1)s} - u_{ns})^3} - (V_{(n)(n+1)})^2\frac{u_{n+1} - u_n}{(r_n + u_{ns} - u_{(n+1)s})^2}\Big] \quad (13)$$

$$w_n'''' + \alpha_3\ddot{w}_n - \alpha_3\Big[2\alpha_1\Gamma(u_{ns},u_n) + 2\alpha_2\Gamma(w_{ns},w_n)\Big]w_{ns}'' - \alpha_3\Big[N_n + \alpha_1\Gamma(u_{ns},u_{ns}) + \alpha_2\Gamma(w_{ns},w_{ns})\Big]w_n'' = (2\beta_g + \beta_{3g}(1-w_{ns})^3)w_n\frac{(V_{(n)g})^2}{(1-w_{ns})^3} + \alpha_{2g}[(V_{(n)(n-1)})^2 (w_{(n-1)} - w_n) + (V_{(n)(n+1)})^2(w_{(n+1)} - w_n)] \quad (14)$$

2.3 Reduced-Order Model

In order to obtain reduced order model equations, we apply Galerkin method to Eqns. (11), (12), (13) and (14). Considering single mode approximation, the static and dynamic deflection of the beam along both the directions can be assumed as:

$$\begin{gathered}
u_{ns}(x) = q_{n1}(y,z)\phi(x),\ u_{(n-1)s}(x) = q_{(n-1)1}(y,z)\phi(x), u_{(n+1)s}(x) = q_{(n+1)1}(y,z)\phi(x),\\
w_{ns}(x) = q_{n2}(y,z)\phi(x),\ w_{(n-1)s}(x) = q_{(n-1)2}(y,z)\phi(x),\ w_{(n+1)s}(x) = q_{(n+1)2}(y,z)\phi(x),\\
u_n(x,t) = P_{n1}(t)\phi(x),\ u_{n-1}(x,t) = P_{(n-1)1}(t)\phi(x),\ u_{n+1}(x,t) = P_{(n+1)1}(t)\phi(x),\\
w_n(x,t) = P_{n2}(t)\phi(x),\ w_{n-1}(x,t) = P_{(n-1)2}(t)\phi(x),\ w_{n+1}(x,t) = P_{(n+1)2}(t)\phi(x).
\end{gathered}$$

where, $\phi(x)$ is the linear undamped approximate mode shape for the fixed-fixed beam, q is the static deflection and $P(t)$ is the non-dimensional modal co-ordinate. Assuming the linear undamped approximate mode shape for fixed-fixed beam as $\phi(x) = \sqrt{(\frac{2}{3})}\Big(1 - \cos(2\pi x)\Big)$ such that $\int_0^1(\phi_1(x))^2dx = 1$ [18]. Substituting it into static equations given by Eqns. (11) and(12) and then applying Galerkin method, the static equations reduced to a set of non-linear algebraic equations as

$$\frac{16}{9}\pi^4\alpha_1 q_{n1}^3 + \Big(\frac{16}{3}\pi^4 + \frac{16}{9}\pi^4\alpha_2 q_{n2}^2 + \frac{4}{3}\pi^2 N_n\Big)q_{n1} - \beta_s\Bigg[\frac{V_{(n-1)(n)}^2}{r_{n-1}^2}\sqrt{\frac{2/3}{(1 + 2\sqrt{\frac{2}{3}}\frac{(q_{(n-1)1} - q_{(n)1})}{r_{n-1}})^3}} - \frac{V_{(n)(n+1)}^2}{r_n^2}\sqrt{\frac{2/3}{(1 + 2\sqrt{\frac{2}{3}}\frac{(q_{n1} - q_{(n+1)1})}{r_n})^3}}\Bigg] = 0 \quad (15)$$

$$\frac{16}{9}\pi^4\alpha_2 q_{n2}^3 + \left(\frac{16}{3}\frac{\pi^4}{\alpha_4} + \frac{16}{9}\pi^4\alpha_1 q_{n1}^2 + \frac{4}{3}\pi^2 N_n\right)q_{n2} - \frac{\beta_g}{\alpha_3}V_{(n)(g)}^2\sqrt{\frac{2/3}{(1-2\sqrt{\frac{2}{3}}q_{n2})^3}} - \frac{\sqrt{6}}{3}\frac{\beta_{2g}}{\alpha_3}$$
$$V_{(n)(g)}^2 + \frac{\sqrt{6}}{3}\frac{\beta_{3g}}{\alpha_3}V_{(n)(g)}^2 + \frac{\beta_{3g}}{\alpha_3}V_{(n)(g)}^2 q_{n2} + \frac{\sqrt{6}}{3}\frac{\alpha_g}{\alpha_3}[V_{(n)(n-1)}^2 + V_{(n+1)(n)}^2] + \frac{\alpha_{2g}}{\alpha_3}$$
$$\left(V_{(n)(n-1)}^2 q_{(n-1)2} - [V_{(n)(n-1)}^2 + V_{(n+1)(n)}^2]q_{n2} + V_{(n+1)(n)}^2 q_{(n+1)2}\right) = 0. \quad (16)$$

On solving the above equations, we get static deflections q_n. Similarly, after substituting the assumed form of static and dynamic deflections from Eqns. (13) and (14) and then applying Galerkin method, we get the reduced form of modal dynamic equation as:

$$\ddot{P}_{n1}(t) + \lambda_{n1}P_{n1}(t) + c_{n(n+1)i}P_{(n+1)1}(t) + c_{n(n-1)i}P_{(n-1)1}(t) + c_{nio}P_{n2}(t) = 0 \quad (17)$$
$$\ddot{P}_{n2}(t) + \lambda_{n2}P_{n2}(t) + c_{n(n+1)o}P_{(n+1)2}(t) + c_{n(n-1)o}P_{(n-1)2}(t) + c_{noi}P_{n1}(t) = 0. \quad (18)$$

Rewriting the equation in the matrix form, as $\ddot{P} + [M]P = 0$, we obtain a generalized equation for N-beam system, where, P is given by $[P] = [P_{11},\ P_{12}, ...,\ P_{k1},\ P_{k2}, ...,\ P_{N1}, P_{N2}]^T$ and matrix M is given by

$$M = \begin{bmatrix}
\lambda_{11} & c_{1io} & c_{12i} & 0 & ... & . & . & . & . & . & 0 & 0 \\
c_{1oi} & \lambda_{12} & 0 & c_{12o} & ... & . & . & . & . & . & 0 & 0 \\
. & & & & & & & & & & . & . \\
. & & & & & & & & & & . & . \\
. & & & ... & c_{n(n-1)i} & 0 & \lambda_{n1} & c_{nio} & c_{n(n+1)i} & ... & . & . \\
. & & & ... & c_{(n-1)no} & c_{noi} & \lambda_{n2} & 0 & c_{(n+1)no} & ... & . & . \\
. & & & & & & & & & & . & . \\
. & & & & & & & & & & . & . \\
0 & . & . & . & . & . & . & ... & c_{N(N-1)i} & 0 & \lambda_{N1} & c_{Nio} \\
0 & . & . & . & . & . & . & ... & 0 & c_{(N-1)No} & c_{Noi} & \lambda_{N2}
\end{bmatrix}. \quad (19)$$

where, $n = 1,\ 2,\ ....,\ N$ and λ_{n1}, λ_{n2}, c_{nio}, $c_{n(n-1)i}$, $c_{n(n+1)i}$, c_{noi}, $c_{n(n-1)o}$, and $c_{n(n+1)o}$ are uncoupled and coupled coefficients which are given by Eqn. (20) to Eqn. (23)

$$\lambda_{n1} = \left[\frac{16}{3}\pi^4 + \frac{16}{9}\pi^4\alpha_2 q_{n2}^2 + \frac{16}{3}\pi^4\alpha_1 q_{n1}^2 + \frac{4}{3}\pi^2 N_n - 2\beta_s\left(\frac{V_{(n)(n-1)}^2}{r_{n-1}^3(1-2\sqrt{\frac{2}{3}}\frac{(q_{n1}-q_{(n-1)1})}{r_{n-1}})^{\frac{5}{2}}}\right.\right.$$
$$\left.\left. + \frac{V_{(n)(n+1)}^2}{r_n^3(1-2\sqrt{\frac{2}{3}}\frac{(q_{(n+1)1}-q_{n1})}{r_n})^{\frac{5}{2}}}\right)\right], \quad (20)$$

$$\lambda_{n2} = \left[\frac{16}{3}\frac{\pi^4}{\alpha_4} + \frac{16}{9}\pi^4\alpha_1 q_{n1}^2 + \frac{16}{3}\pi^4\alpha_2 q_{n2}^2 + \frac{4}{3}\pi^2 N_n - 2\frac{\beta_g}{\alpha_3}V_{(n)(g)}^2(1-2\sqrt{\frac{2}{3}}q_{n2})^{-\frac{5}{2}}\right.$$
$$\left. - \frac{\beta_{3g}}{\alpha_3}V_{(n)(g)}^2 + \frac{\alpha_{2g}}{\alpha_3}(V_{(n)(n-1)}^2 + V_{(n+1)(n)}^2)\right], \quad (21)$$

$$c_{n(n-1)i} = 2\beta_s\left(\frac{V^2_{(n-1)n}}{r^3_{n-1}(1-2\sqrt{\frac{2}{3}}\frac{(q_{n1}-a_{(n-1)1}}{r_{n-1}})^{\frac{5}{2}}}\right),\ c_{n(n+1)i} = 2\beta_s\left(\frac{V^2_{(n)(n+1)}}{r^3_{n}(1-2\sqrt{\frac{2}{3}}\frac{(q_{(n+1)1}-q_{n1}}{r_{n}})^{\frac{5}{2}}}\right), \quad (22)$$

$$c_{nio} = \frac{32}{9}\alpha_2 q_{n1}q_{n2}\pi^4,\ c_{n(n-1)o} = \frac{\alpha_{2g}}{\alpha_3}V^2_{(n)(n-1)},\ c_{noi} = \frac{32}{9}\alpha_1 q_{n1}q_{n2}\pi^4,\ c_{n(n+1)o} = \frac{\alpha_{2g}}{\alpha_3}V^2_{(n+1)(n)}. \quad (23)$$

Here, i and o denote two different modes, say, in-plane and out-of-plane modes, λ_{n1} and λ_{n2} correspond to the unperturbed natural frequencies of the n^{th} beam of i and o modes,respectively. c_{nio} denotes modal coupling of i and o modes of n^{th} beam, $c_{n(n-1)i}$ and $c_{n(n+1)i}$ denote interaction of i mode adjacent beams. Similarly, $c_{n(n-1)o}$ and $c_{n(n+1)o}$ denote interaction of o mode of adjacent beams. Finally, the frequencies corresponding to different modes for each beam can be found from the square root of the eigenvalues of matrix $[M]$. Consequently, for N beams, there are $2N$ modes and the frequencies of $2N$ modes of an array of N beams can be tuned using different initial tensions N, fringing coefficients and variable gaps between beams and electrodes .

3 Results and Discussion

In this section, we first validate our mathematical model with the experimental results for single beam and an array of three beams from [19]. The beams are fabricated on a bulk-micromachined silicon die with suspended membrane of size 500μm$\times 500\mu$m using standard micromachining process [7]. It involves many substeps such as deposition of photoresist from spinning process, tranfer of pattern using e-beam lithography and its development, thermal deposition of AuPd alloy, and finally, dry etching to get suspended structure of single beam or multibeams array. The dimensions of fabrication structure can be measured using surface profiler. However, due to variation in current and voltage of e-beam under a given magnification, beam width as well as interbeam gaps may also change. Additionally, the plane of suspended beams may also found to be little different from the top surface of substrate due to twisting or bending of some of the beams subjected to thermal stresses. Therefore, to account such variation, we identify geometric (interbeam gaps) and electric field parameters (k_1, k_2, and k_3) by comparing the results from developed model with measured frequencies at different DC voltages. Since the ac voltage is in the range of 1-40 mV corresponding to DC bias of 0-90 V, the response is considered to be in the linear regime [19].

In this paper, we take the same dimension of all the beams in an array. Here, each beam is having a length of $L = 500\ \mu$m, width, $B = 4\ \mu$m, height, $H = 200$ nm and is separated from the bottom electrode by a gap of $d = 500\ \mu$m. A possible variation in beam width and gap between the beams are captured by taking effective gap between the beams, g_i, in the range of 1 μm to 7 μm. Since the elastic modulus, E, and density, ρ, of beam are dependent on the composition of AuPd alloy, and initial tension, N_0, in the beam depends on the thermal deposition process as well as heating due to laser, we compute these properties by comparing the experimental and theoretical results corresponding to frequencies at zero DC voltage, i.e., $V_{dc} = 0$, and the values corresponding to crossing region.

3.1 Single Beam

In this case, a fixed-fixed beam is separated from two side electrodes and bottom electrode. Consequently, since the side neighbours of the single beam is fixed, the coupling of either modes of the beam with the side electrode are zero, i.e., $c_{n(n-1)i} = c_{n(n+1)i} = c_{n(n-1)o} = c_{n(n+1)o} = 0$. For $N = 1$, the size of P and M are 2×1 and 2×2. The coefficients $\lambda_{n1},$, λ_{n2}, c_{nio}, and c_{noi} are the only non-zero terms in matrix M as given by Eqn. (19). On comparing the analytical model with experimental results [19], for $E = 2.484 \times 10^{10}\text{N/m}^2$, $\rho = 3227.4$ kg/m^3, $N_0 = 35.86$ μN/m, we obtain the forcing coefficients of $k_1 = 0.97$, $k_2 = 2.2$ and $k_3 = 1.5$ when the gaps between the beam and the side electrodes are given by $g_0 = 4.5$ μm and $g_1 = 7$ μm, respectively. Taking the corresponding values of non-dimensional gap ratio $r_0 = 1$ and $r_1 = 1.55$, we show the comparison of analytical and experimental values of the in-plane and out-of-plane frequencies at different dc voltages for single beam in Figure 3(a). As the dc voltage increases from 0 to 90V between side electrode and the beam, in-plane frequency decreases with the dc voltage and, thus, showing the softening effect. Due to large dc voltage along in-plane direction, the beam undergoes large deflection which leads to mid-plane stretching of the beam. Since, the gap $d = 500$ μm between the beam and bottom electrode is more than 100 times the gap between the beam and side electrode, g_0, the influence of direct forcing between beam and bottom electrode is negligible. It is found that the motion corresponding to out-of-plane mode is mostly influenced by fringing forces. Therefore, the tension induced due to mid-plane stretching of beam along in-plane direction dominates over the electrostatic forces in out-of-plane direction. Consequently, the frequency corresponding to out-of-plane mode increases as dc voltage increases. Due to decrease in the frequency of in-plane mode and increase in the frequency of out-of-plane mode, both modes cross over at around dc voltage of 81 V and show coupling. The coupling of modes are identified by the non-zero width of coupled region. However, the mode coupling at frequency crossing disappears when the gaps between the beam and the side electrodes are the same due to equal and opposite forces acting on the beam along the in-plane direction. We also noticed that the frequency crossing can be tuned by fringing forces from the side electrodes in z-direction. Although, the frequency tuning of in-plane and out-of-plane mode can be further achieved beyond the coupling region by increasing the DC voltage as shown in Figure 4(a), it is limited by the pull-in instability corresponding to in-plane mode. The theoretical value of pull-in voltage is found to be around 205 V. Now,we study the frequency tuning of three beams array.

3.2 An Array of Three Beams

To validate the model developed in the paper for multibeams array and present further analysis, we take an array of three beams. In this case, $N = 3$ and the size of P and M become 6×1 and 6×6. We compare the frequencies obtained from the resulting matrix M with experimental results [19] by tunning with initial tension, gap thickness, fringing forces, etc., for $E = 3.183 \times 10^{10}$, N/m^2, $\rho = 3234.2$ kg/m^3, $N_0 = 43.81$ μN/m. Figure 3(b) shows the comparison of in-plane and out-of-plane frequencies with DC voltage for three different beams with experimental results. The results are obtained by, first, tuning the initial tensions $N_1 = N_0$, $N_2 = 1.06N_0$, $N_3 = 1.13N_0$ at zero DC voltage, and, then, the fringing field parameters at large dc voltage corresponding to crossing region as $k_1 = 0.132,\ 0.45,\ 1$, $k_2 = 1,\ 1,\ 1$ and $k_3 = 2.5,\ 3,\ 2.5$ for the three beams which are separated from each other as $g_0 = 2$ μm, $g_1 = 2.7$ μm, $g_2 = 4.9$ μm, and $g_3 = 4.5$ μm,

respectively. Unlike the single beam, we also observe frequency crossings between the modes of adjacent beams and those of non-adjacent beams. While the frequency crossing between non-adjacent beams does not show any coupling, the frequency crossing between adjacent beam shows coupling. We also noticed that the coupling strength of the modes of side beams is very low as compared to that of the middle beam, probably, due to a non-uniform gap between the middle beam and the two side beams.

It is also observed that by changing the initial tension from N_0 to $1.06N_0$ and $1.13N_0$, the frequency shift of about 5 kHz and 10 kHz can be obtained corresponding to out-of-plane modes of three beams array at zero DC voltage. Such tuning in initial tension increases the frequency bandwidth by 18.5 kHz due to frequency tuning of in-plane and out-of plane corresponding to DC bias of 80 V. Thus, the given array is found to be very sensitive to initial tension. Although, the frequency tuning of different modes can be achieved beyond the crossing region by increasing the DC voltage as shown in Figure 4(b), it is limited by pull-in effect corresponding to in-plane mode of first beam of the array. In the present case, we found the theoretical pull-in voltage corresponding to in-plane motion of first beam in three beam array as 149 V. It is also noticed that the pull-in voltage would have been around 120 V if the first beam would have been operated as a single entity. Therefore, the modal coupling of different modes of three beams array increases the stable response as well as frequency bandwidth by increasing the pull-in voltage. Now, we study the influence of various factors such as interbeam gap, electric field parameters, and initial tension on the frequency tuning of an array of three beams.

3.3 Tuning of Modal Frequencies and Coupling Regions

In this section, we demonstrate the tuning of modal frequencies and coupling regions by varying initial tensions, gap between the beams and bottom electrode, gaps between the beam and side electrodes, and the fringing force coefficients in an array of three beams. To distinguish different modes of same beam, we label in-plane mode as I and out-of-plane mode as O. Three beams in array are marked by $B1$, $B2$, and $B3$. To identify in-plane mode of first beam and out-of-plane mode of second beam, notations $IB1$ and $OB2$ can be used. We also state that the coupling strength of two modes can be identified by width of crossing or anti-crossing regions of two modes.

Taking the same physical properties as mentioned in the previous section, we first show the influence of direct forces between the beams and bottom electrode by taking the gap between beams and bottom electrode as $d = 15\mu$m. Figure 5(a) shows the tunning of modal frequencies and coupling regions under this condition when the initial tension of the beams are $N_1 = N_0$, $N_2 = 1.04N_0$, and $N_3 = 1.05N_0$, the interbeam gaps as $g_0 = 2\mu$m, $g_1 = 2.7\mu$m, $g_2 = 4.9\mu$m, $g_3 = 4.5\mu$m, and the fringing coefficients as $k_1 = 0.135,\ 0.45,\ 1$, $k_2 = 1,\ 1,\ 1$ $k_3 = 2.5,\ 4,\ 2.5$. The variation of the frequencies shows a wider coupling region between modes $OB1$ and $OB2$ at around DC voltage 35 V. We can observed different coupling of same beam as well as adjacent beams. Additionally, we also found that the coupling between the two modes of non-adjacent beams is very weak due non-uniform gaps between the beam and side electrodes. When we consider the same tension in all beams, i.e., $N_1 = N_2 = N_3 = N_0$, we get less numbers of coupling regions as shown in Figure 5(b).

We show the variation of modal frequencies with DC voltage when the fringing field forces are dominant corresponding to large values of gap between the beam and bottom electrodes.

Taking $d = 5000\mu$m and all other parameters same as the previous case, the fringing field effects dominate the direct field effects. Figure 6(a) shows such variation for the beams with different initial tension as $N_1 = N_0$, $N_2 = 1.04N_0$, $N_3 = 1.05N_0$. Figure 6(b) shows the variation when the initial tensions are equal, i.e., $N_1 = N_2 = N_3 = N_0$. Comparison of results show that the mid-plane stretching effect dominates over electrostatic effects when the gap between bottom electrode and beams increases. Similarly, to show the effect of airgaps between interbeam spacing and side electrodes on frequency tuning, we take $g_0 = 2.2\mu$m, $g_1 = 3\mu$m, $g_2 = 5\mu$m, $g_3 = 5.5\mu$m so as to have unequal gaps on either side of each beams. Taking $k_1 = 0.1,\ 0.6,\ 1$, $k_2 = 1,\ 1,\ 1$ and $k_3 = 4,\ 4,\ 3$ and the gap between beams and bottom electrode as $d = 20\mu$m, Figure 7(a) and (b) show tuning of modal frequencies of three beams with different initial tensions $N_1 = N_0$, $N_2 = 1.06N_0$, $N_3 = 1.07N_0$ and same initial tensions, $N_1 = N_2 = N_3 = N_0$, respectively.

Finally, to show the effect of initial tension and number of elements in an array, we consider arrays of 10 beams, 20 beams and 39 beams. In all the cases, the side gap g_n varies from 4 to 5 μm, $k_1 = 1$, $k_2 = 2.5$, $k_3 = 3$, $d = 500$ μm, $L = 500$ μm, $B = 4$ μm, $H = 200$ nm, $E = 3.183 \times 10^{10}$, N/m^2, $\rho = 3234.2$ kg/m^3, $N_0 = 43.81$ μN/m, respectively. Figure 8(a) shows the variation of in-plane and out-of-plane modal frequencies for an array of 10 beams with initial tension, N_n. When N_n vary from N_0 to $1.019N_0$, we get frequency bandwidth of around 13.8 kHz at DC voltage of 80 V. Figure 8(b) shows the frequency variation of modal frequencies for an array of 20 beams with the initial tension N_n varying from N_0 to $1.039N_0$. It shows a frequency bandwidth of around 15.2 kHz at 80 V DC bias. Similarly, Figure 8(c) shows the frequency tuning of two modes of 39 beams in an array with the initial tension N_n varying from $1.08N_0$ to $1.11N_0$. In this case, a frequency bandwidth of 17.5 kHz is observed at DC bias of 80 V.

In short, at a given DC voltage of 80 V, the frequency bandwidth of 13.8 kHz, 15.2 kHz, and 17.5 kHz can be obtained in arrays of 10, 20 and 39 beams when the initial tension vary over the range of $N_0 - 1.019N_0$, $N_0 - 1.039N_0$, and $1.08N_0 - 1.11N_0$, respectively. Additionally, further increase in the bandwidth can also be observed by increasing DC bias beyond 80 V, however, they are also limited by pull-in effect corresponding to a particular mode of the beam in an array. In the present case, the pull-in voltage is found to be much away from the coupling region. We have also observed that the frequency resolution as well as sensitivity can be increased corresponding to a given DC voltage by increasing the number of beams over a given range of initial tension. For example, for the given range of initial tension N_0 to $1.019N_0$ and frequency range of 1.4 kHz at zero DC voltage, an uniform frequency distribution of 10 or 20 beams in an array may give a frequency resolution of about 0.14 kHz or 0.07 kHz. In addition to sensitivity and bandwidth, by increasing the coupling strength of beam, noise level can also be suppressed due to noise squeeze phenomena. Thus, it can increase the dynamic range of the such devices.

4 Conclusions

In this paper, we have presented the tuning of in-plane and out-of-plane modal frequencies and their coupling regions in arrays of fixed-fixed beams by varying side gaps, bottom gap, fringing forces and initial tensions. To do the analysis, first, we obtained the static and dynamic partial differential equations of in-plane and out-of-plane motions of N fixed-fixed beams separated from the side electrodes and bottom electrode under the influence of direct and fringing field electrostatic forces. Taking the transverse deflection of the beam in in-plane and out-of-plane

modes as single mode approximation, we employ Galerkin's method to get nonlinear reduced order static equations and linear dynamic equations. Later, we validate our mathematical model with the experimental results for a single beam and an array of three beams. Finally, we show that by varying the side gaps, bottom gap, fringing coefficients and initial tensions in an array of three beams, we can control the frequency tuning and coupling regions, effectively. Since the arrays are very sensitive to initial tension, the sensitivity of arrays can be increased by increasing the number of elements for a given bandwidth. The bandwidth can be increased by tuning due to DC voltage. However, the range of frequency tuning is limited by the pull-voltage. The pull-in voltage also increases due to modal coupling of different beams of an array.

Acknowledgement

This research is supported in part by the Council of Scientific and Industrial Research (CSIR), India (22(0696)/15/EMR-II). The authors also acknowledge useful discussions on MEMS arrays with Prof. Oded Gottlieb and Prof. Eyal Buks of Technion-Israel Institute of Technology, Israel.

References

[1] Suzuki, N., Tanigawa, H., and Suzuki, K., 2013, "Zeptogram-scale nanomechanical mass sensing," Journal of Micromechanics and microengineering, **23**, pp. 045018-045030.

[2] Spletzer, M., Raman, A., Sumali, H., and Sullivan, J. P., 2008, "Highly sensitive mass detection and identification using vibration localization in coupled microcantilever arrays," Applied Physics Letters, **92**, pp. 0114102.

[3] Hopcroft, M. A., Kim, B., Chandorkar, S., Melamud, R., Agarwal, M., Jha, C. M., Bahl, G., Salvia, J., Mehta, H., Lee, H. K., Candler, R. N., and Kenny, T. W., 2007, "Using the temperature dependence of resonator quality factor as a thermometer," Applied Physics Letters, **91**, pp. 013505.

[4] Verbridge, S. S., Shapiro, D. F., Craighead, H. G., and Parpia, J. M., 2007, "Macroscopic tunning of nanomechanics:substrate bending for reversible control of frequency and quality factor of nanostring resonators," Nano Letters, **7** (6), pp. 1728-1735.

[5] Pandey, A. K., Gottlieb, O., Shtempluck O., and Buks, E., 2006, "Performance of an AuPd micromechanical resonator as a temperature sensor," Applied Physics Letters, **96**(20), pp. 203105-1-203105-3.

[6] Remtema, T., and Lin, L., 2001, "Active frequency tunning for micro resonators by localized thermal stressing effects," Sensors and Actuators A, Physical, **91**, pp. 326.

[7] Buks, E., and Roukes, M. L., 2002, "Electrically tunable collective response in a coupled micromechanical array," IEEE Journal of Microelectromechanical Systems, **11**, pp. 802-807.

[8] Kozinsky, I., Postma, H. W. Ch., Bargatin, I., Roukes, M. L., 2006, "Tuning nonlinearity, dynamic range, and frequency of nanomechanical resonators," Applied Physics Letters, **88**, pp. 253101–3.

[9] Solanki, H. S., Sengupta, S., Dhara, S., Singh, V., Patil, S., Dhall, R., Parpia, J., Bhattacharya, A., and Deshmukh, M. M., 2010, " Tuning mechanical modes and influence of charge screening in nanowire resonators," Physical Reviews B, **81**, pp. 115459.

[10] Pandey, A. K., Venkatesh, K. P., Pratap, R., 2009, "Effect of metal coating and residual effect on the resonant frequency of MEMS resonators," Sadhana, **34**, pp. 651-662.

[11] Huang, X. M. H., Manolidis, M., Jun, S. C., and Hone, J., 2005, "Nanomechanical hydrogen sensing," Applied Physics Letters, **86**, pp. 143104.

[12] Zalalutdinov, M. K., Baldwin, J. W., Marcus, M. H., Reichenbach, R. B., Parpia, J. M., and Houston, B. H., 2006, "Two-dimensional array of coupled nanomechanical resonators," Applied Physics Letters, **88**, pp. 143504.

[13] Krylov, S., Lulinsky,S., Ilic,B. R., and Schneider, I., 2014, "Collective dynamics and pattern switching in an array of parametrically excited microcantilevers interacting through fringing electrostatic fields," Applied Physics Letters, **105**, pp. 071909.

[14] Thijssen, R., Kippenberg, T. J., Polman, A., and Verhagen, E., 2014, "Parallel transduction of nanomechanical motion using plasmonic resonators," ACS Photonics, **1**, pp. 1181.

[15] Kambali, P. N., and Pandey, A. K., 2015, "Nonlinear response of a microbeam under combined direct and fringing field excitation," Journal Computational and Nonlinear Dynamics, **10**, pp. 051010.

[16] Gutschmidt, S., and Gottlieb, O., 2012 , "Nonlinear dynamic behavior of a microbeam array subject to parametric actuation at low, medium and large DC-voltages," Nonlinear Dynamics, **67**, pp. 1-36.

[17] Gutschmidt, S., and Gottlieb, O., 2010 , "Internal resonance and bifurcations of an array below the first pull-in instability," International Journal of Bifurcation and Chaos, **20**, pp. 605-618.

[18] Pandey, A. K., 2013, "Effect of coupled modes on pull-in voltage and frequency tuning of a NEMS device," Journal of Micromechanics and Microengineering, **23**(8), pp. 085015-1-085015-10.

[19] Kambali, P. N., Swain, G., Pandey, A., K., Buks, E., and Gottlieb, O., 2015, "Coupling and tuning of modal frequencies in direct current biased microelectromechanical systems arrays," Applied Physics Letters, **107**, pp. 063104.(Supplementary material at http://dx.doi.org/10.1063/1.4928536)

[20] Leamy, M. J., and Gottlieb, O., 2000, "Internal resonances in whirling strings involving longitudinal dynamics and material non-linearities," Journal of Sound and Vibration , **236** (4), pp. 683-703.

List of Figures

1 (a) Side view of N fixed-fixed beams of width B, thickness H are separated from the side electrodes, E_1 and E_2, and the ground electrode E_g by distance d; (b) Top view of N beams and each having a length of L. Here, i^{th} beam is separated from its neighboring beams by gaps of g_{i-1} and g_i, respectively. 14

2 (a) Displacement of the beam in two different directions are represented by y and z; (b) The corresponding forces are represented by Q_z and Q_y. 15

3 Comparison of experimental and analytical results for (a) single beam with gap ratios $r_0 = 1$ and $r_1 = 1.55$ and (b) three beam arrays with gap ratios $r_0 = 1$, $r_1 = 1.35$, $r_2 = 2.45$, and $r_3 = 2.25$. Here, $r_n = \frac{g_n}{g_0}$, $n = 0...N$. 16

4 Variation of in-plane and out-of-plane frequencies with DC bias beyond crossing region of (a) single beam and (b) an array of three beams. 17

5 Tuning of frequencies of two modes and coupling regions in an array of three beams with $g_0 = 2\mu$m, $g_1 = 2.7\mu$m, $g_2 = 4.9\mu$m, $g_3 = 4.5\mu$m, $k_1 = 0.135, 0.45, 1$, $k_2 = 1, 1, 1$ $k_3 = 2.5, 4, 2.5$ (a) for $N_1 = N_0$,$N_2 = 1.04N_0$, $N_3 = 1.05N_0$ and $d = 15\mu$m. (b) for $N_1 = N_2 = N_3 = N_0$ and $d = 15\mu$m. In both the cases, $L = 500$ μm, $B = 4$ μm, $H = 200$ nm, $E = 3.183 \times 10^{10}$, N/m^2, $\rho = 3234.2$ kg/m^3, $N_0 = 43.81$ μN/m. 18

6 Tuning of frequencies of two modes and coupling regions in an array of three beams with $g_0 = 2\mu$m, $g_1 = 2.7\mu$m, $g_2 = 4.9\mu$m, $g_3 = 4.5\mu$m, $k_1 = 0.135, 0.45, 1$, $k_2 = 1, 1, 1$ $k_3 = 2.5, 4, 2.5$. (a) for $N_1 = N_0$,$N_2 = 1.04N_0$, $N_3 = 1.05N_0$ and $d = 5000\mu$m. (b) for $N_1 = N_2 = N_3 = N_0$ and $d = 5000\mu$m. In both the cases, $L = 500$ μm, $B = 4$ μm, $H = 200$ nm, $E = 3.183 \times 10^{10}$, N/m^2, $\rho = 3234.2$ kg/m^3, $N_0 = 43.81$ μN/m. 19

7 Tuning of frequencies of two modes and coupling regions in an array of three beams with $g_0 = 2.2\mu$m, $g_1 = 3\mu$m, $g_2 = 5\mu$m, $g_3 = 5.5\mu$m, $k_1 = 0.1, 0.6, 1$, $k_2 = 1, 1, 1$ $k_3 = 4, 4, 3$, $d = 20\mu$m (e) for $N_1 = N_0$,$N_2 = 1.06N_0$, $N_3 = 1.07N_0$. (f) for $N_1 = N_2 = N_3 = N_0$. In bothl the cases, $L = 500$ μm, $B = 4$ μm, $H = 200$ nm, $E = 3.183 \times 10^{10}$, N/m^2, $\rho = 3234.2$ kg/m^3, $N_0 = 43.81$ μN/m. 20

8 Tuning of frequencies of two modes and coupling regions with g_n varying from 4 to $5\mu m$, $k_1 = 1$, $k_2 = 2.5$ $k_3 = 3$, $d = 500\mu$m (a) for an array of 10 beam, with initial tension N_n varying N_0 to$1.019N_0$, (b) for an array of 20 beam, with initial tension N_n varying N_0 to$1.039N_0$, and (c) for an array of 39 beam,with initial tension N_n varying $1.08N_0$ to$1.11N_0$ .In all the cases, $L = 500$ μm, $B = 4$ μm, $H = 200$ nm, $E = 3.183 \times 10^{10}$, N/m^2, $\rho = 3234.2$ kg/m^3, $N_0 = 43.81$ μN/m. 21

Journal of Vibration and Acoustics. Received September 14, 2015;
Accepted manuscript posted January 21, 2016. doi:10.1115/1.4032517

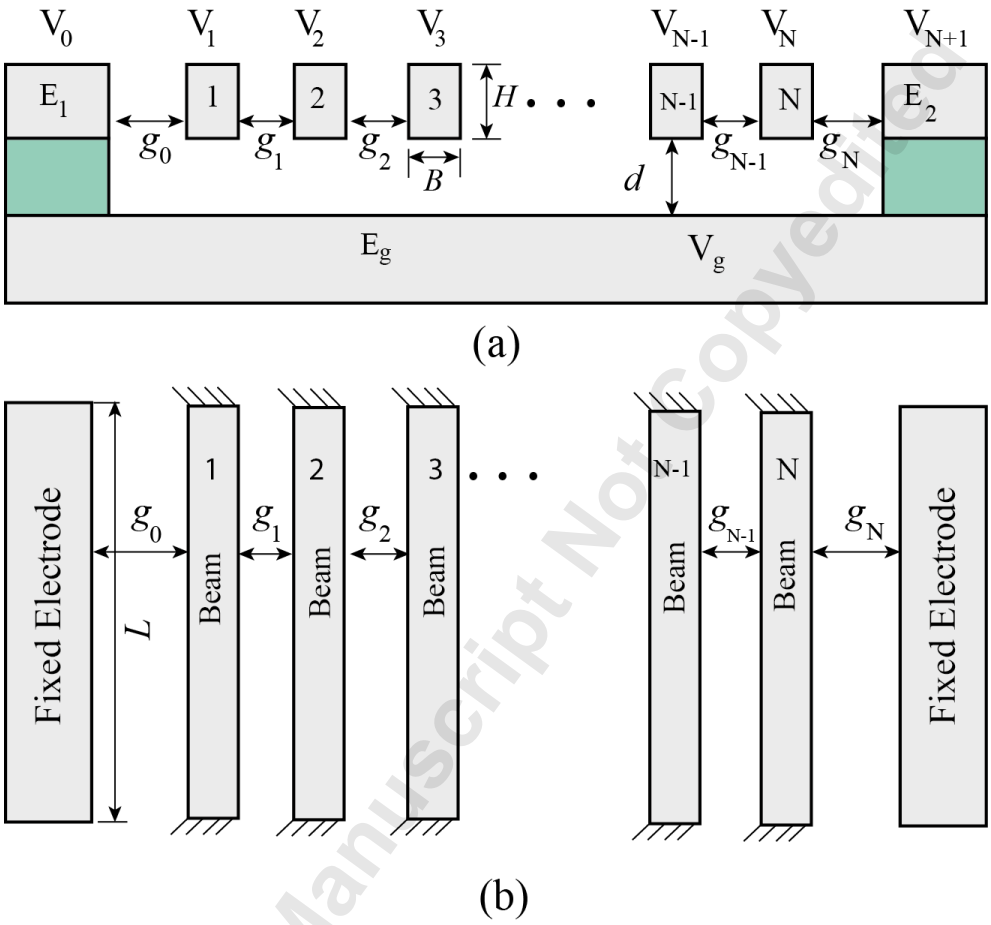

Figure 1: (a) Side view of N fixed-fixed beams of width B, thickness H are separated from the side electrodes, E_1 and E_2, and the ground electrode E_g by distance d; (b) Top view of N beams and each having a length of L. Here, i^{th} beam is separated from its neighboring beams by gaps of g_{i-1} and g_i, respectively.

Journal of Vibration and Acoustics. Received September 14, 2015;
Accepted manuscript posted January 21, 2016. doi:10.1115/1.4032517

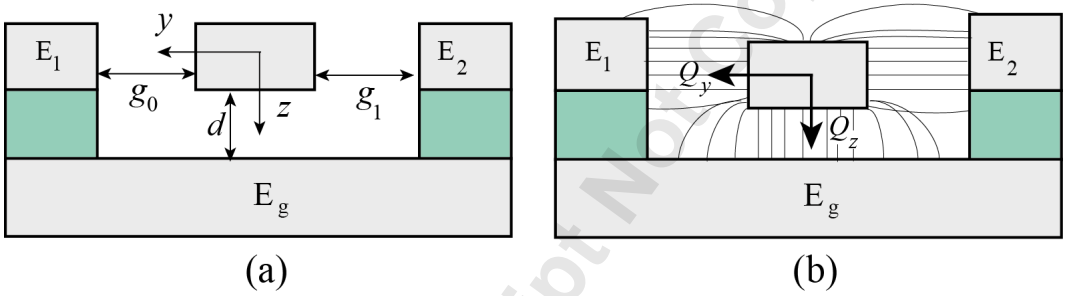

Figure 2: (a) Displacement of the beam in two different directions are represented by y and z; (b) The corresponding forces are represented by Q_z and Q_y.

Journal of Vibration and Acoustics. Received September 14, 2015;
Accepted manuscript posted January 21, 2016. doi:10.1115/1.4032517

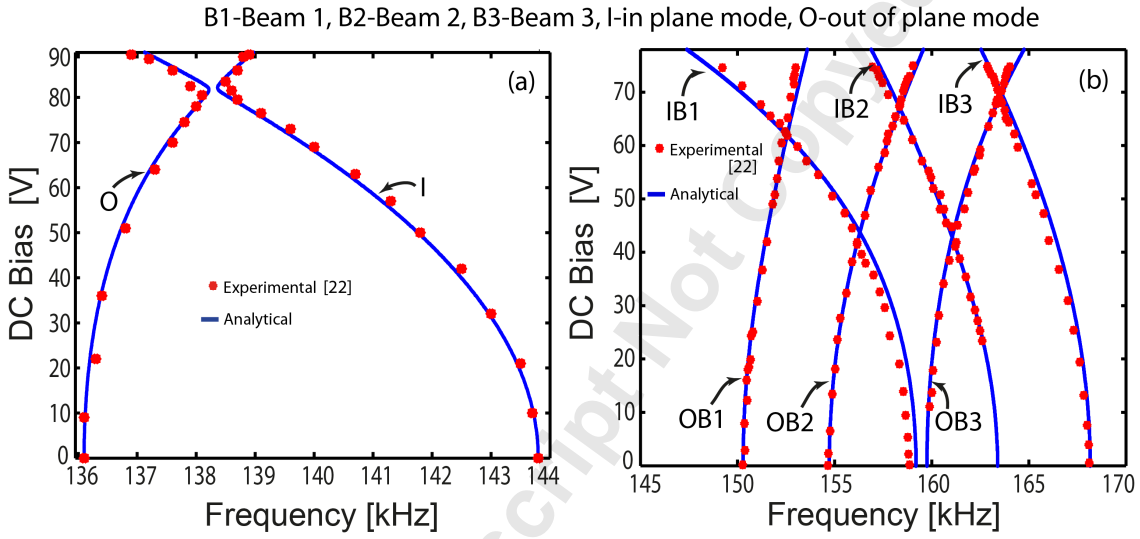

Figure 3: Comparison of experimental and analytical results for (a) single beam with gap ratios $r_0 = 1$ and $r_1 = 1.55$ and (b) three beam arrays with gap ratios $r_0 = 1$, $r_1 = 1.35$, $r_2 = 2.45$, and $r_3 = 2.25$. Here, $r_n = \frac{g_n}{g_0}$, $n = 0...N$.

Journal of Vibration and Acoustics. Received September 14, 2015;
Accepted manuscript posted January 21, 2016. doi:10.1115/1.4032517

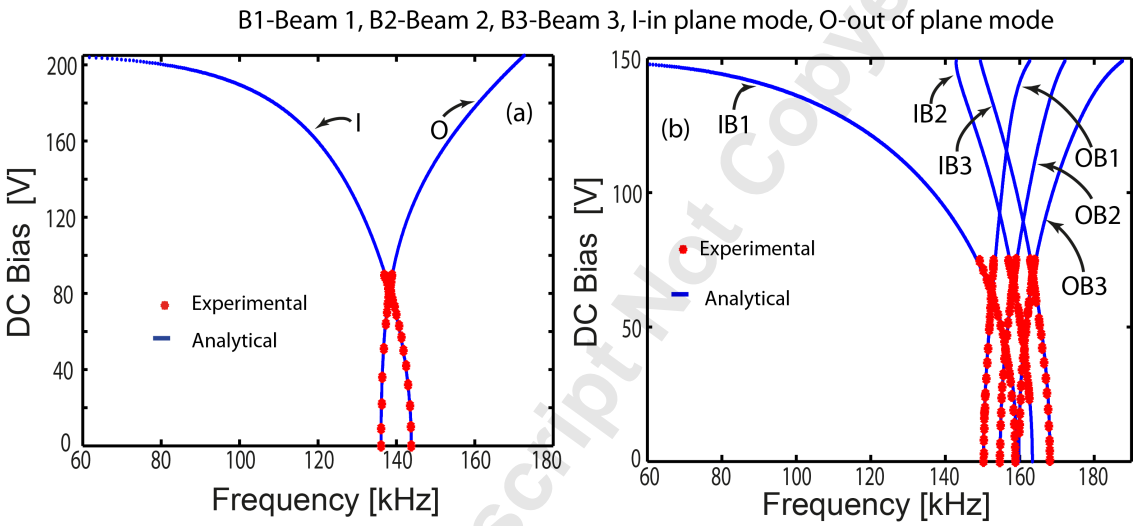

Figure 4: Variation of in-plane and out-of-plane frequencies with DC bias beyond crossing region of (a) single beam and (b) an array of three beams.

Journal of Vibration and Acoustics. Received September 14, 2015;
Accepted manuscript posted January 21, 2016. doi:10.1115/1.4032517

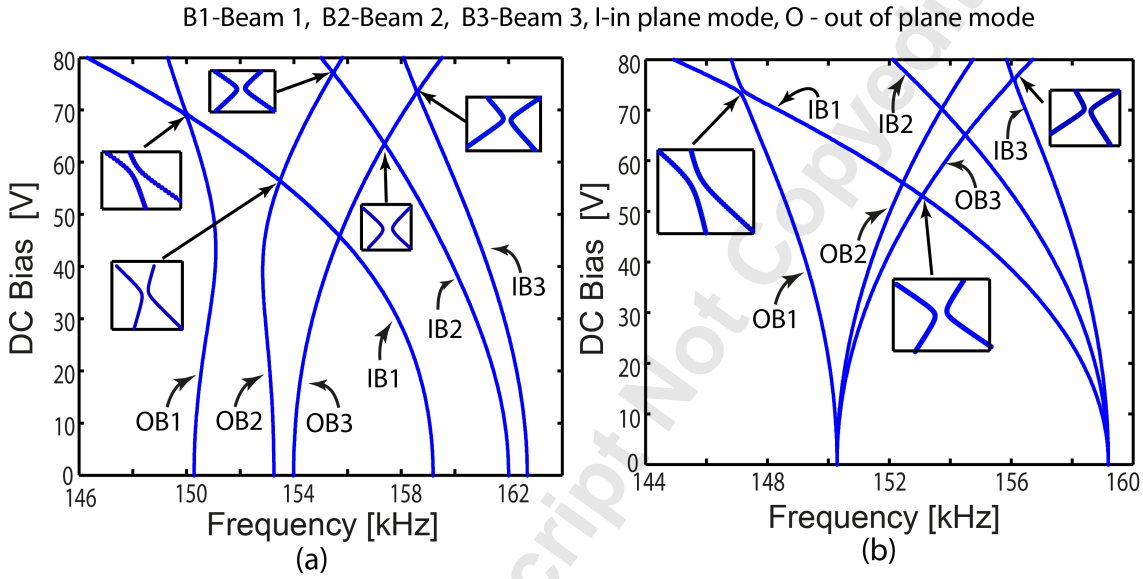

Figure 5: Tuning of frequencies of two modes and coupling regions in an array of three beams with $g_0 = 2\mu$m, $g_1 = 2.7\mu$m, $g_2 = 4.9\mu$m, $g_3 = 4.5\mu$m, $k_1 = 0.135, 0.45, 1$, $k_2 = 1, 1, 1$ $k_3 = 2.5, 4, 2.5$ (a) for $N_1 = N_0$,$N_2 = 1.04N_0$, $N_3 = 1.05N_0$ and $d = 15\mu$m. (b) for $N_1 = N_2 = N_3 = N_0$ and $d = 15\mu$m. In both the cases, $L = 500$ μm, $B = 4$ μm, $H = 200$ nm, $E = 3.183 \times 10^{10}$, N/m^2, $\rho = 3234.2$ kg/m^3, $N_0 = 43.81$ μN/m.

Journal of Vibration and Acoustics. Received September 14, 2015;
Accepted manuscript posted January 21, 2016. doi:10.1115/1.4032517

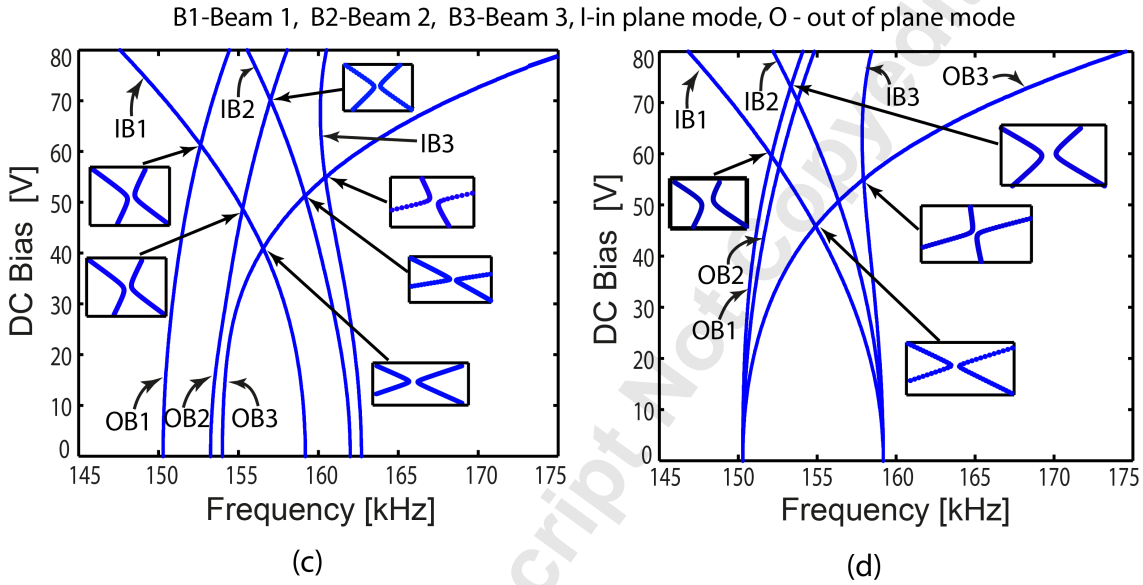

Figure 6: Tuning of frequencies of two modes and coupling regions in an array of three beams with $g_0 = 2\mu$m, $g_1 = 2.7\mu$m, $g_2 = 4.9\mu$m, $g_3 = 4.5\mu$m, $k_1 = 0.135, 0.45, 1$, $k_2 = 1, 1, 1$ $k_3 = 2.5, 4, 2.5$. (a) for $N_1 = N_0$,$N_2 = 1.04N_0$, $N_3 = 1.05N_0$ and $d = 5000\mu$m. (b) for $N_1 = N_2 = N_3 = N_0$ and $d = 5000\mu$m. In both the cases, $L = 500$ μm, $B = 4$ μm, $H = 200$ nm, $E = 3.183 \times 10^{10}$, N/m^2, $\rho = 3234.2$ kg/m^3, $N_0 = 43.81$ μN/m.

Journal of Vibration and Acoustics. Received September 14, 2015;
Accepted manuscript posted January 21, 2016. doi:10.1115/1.4032517

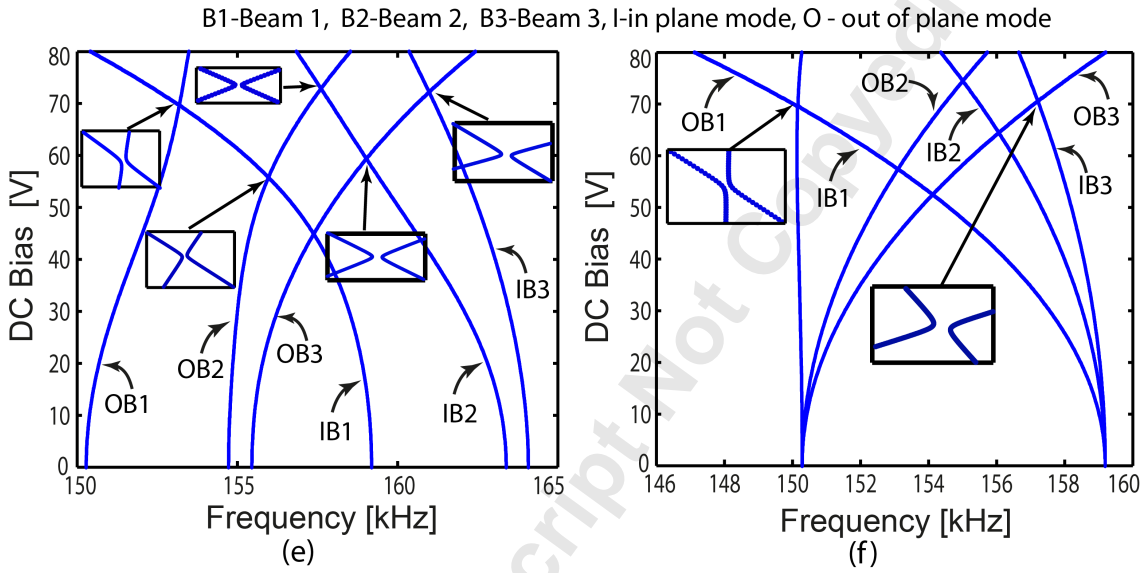

Figure 7: Tuning of frequencies of two modes and coupling regions in an array of three beams with $g_0 = 2.2\mu$m, $g_1 = 3\mu$m, $g_2 = 5\mu$m, $g_3 = 5.5\mu$m, $k_1 = 0.1, 0.6, 1$, $k_2 = 1, 1, 1$ $k_3 = 4, 4, 3$, $d = 20\mu$m (e) for $N_1 = N_0$,$N_2 = 1.06N_0$, $N_3 = 1.07N_0$. (f) for $N_1 = N_2 = N_3 = N_0$. In bothl the cases, $L = 500$ μm, $B = 4$ μm, $H = 200$ nm, $E = 3.183 \times 10^{10}$, N/m^2, $\rho = 3234.2$ kg/m^3, $N_0 = 43.81$ μN/m.

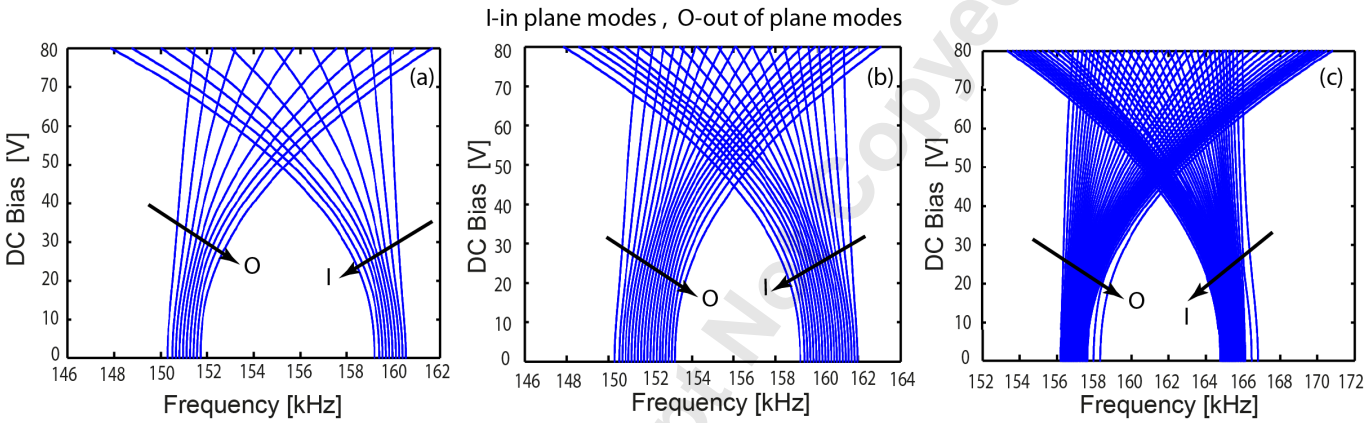

Figure 8: Tuning of frequencies of two modes and coupling regions with g_n varying from 4 to $5\mu m$, $k_1 = 1$, $k_2 = 2.5$ $k_3 = 3$, $d = 500\mu$m (a) for an array of 10 beam, with initial tension N_n varying N_0 to$1.019N_0$, (b) for an array of 20 beam, with initial tension N_n varying N_0 to$1.039N_0$, and (c) for an array of 39 beam,with initial tension N_n varying $1.08N_0$ to$1.11N_0$ .In all the cases, $L = 500$ μm, $B = 4$ μm, $H = 200$ nm, $E = 3.183 \times 10^{10}$, N/m^2, $\rho = 3234.2$ kg/m^3, $N_0 = 43.81$ μN/m.